CHAPTER 2

Combining NMR Spectroscopic Measurements and Molecular Dynamics Simulations to Determine the Orientation of Amphipathic Peptides in Lipid **Bilayers**

B. SCOTT PERRIN JR., a RICHARD W. PASTOR AND MYRIAM COTTEN*b

Introduction 2.1

The combination of solid-state NMR (ssNMR) and molecular dynamics (MD) simulations provides a rich context for the structural, topological, and dynamic studies of peptides in lipid bilayers and the establishment of important structure-function relationships. 1-12 At minimum, they corroborate measured and theoretical properties. Good agreement between methods supports properties from MD that may not have an experimental analogue, or might otherwise be difficult to obtain. If there is disagreement

New Developments in NMR No. 3 Advances in Biological Solid-State NMR: Proteins and Membrane-Active Peptides Edited by Frances Separovic and Akira Naito © The Royal Society of Chemistry 2014 Published by the Royal Society of Chemistry, www.rsc.org

^a Laboratory of Computational Biology, National Heart, Lung and Blood Institute, National Institutes of Health, Bethesda, MD 20892, USA; ^b Department of Chemistry, Hamilton College, Clinton, NY 13323, USA *Email: mcotten@hamilton.edu

between methods, analysis of the MD trajectory or auxiliary calculations guide convergence and reveal weaknesses in one or both methods.

Oriented sample (OS) ssNMR takes advantage of orientational restraints such as the dipolar coupling (DC), chemical shifts (CS), or ²H quadrupolar interactions to determine the orientation of peptides aligned mechanically (e.g. glass plates) or magnetically (e.g. bicelles) in lipid bilayers. 13-16 Two-dimensional separated local field experiments, such as polarization inversion spin exchange at the magic angle (PISEMA) and ¹⁵N-¹H heteronuclear correlation (HETCOR) spectroscopy applied to multiply ¹⁵N-labeled peptides, yield 2D spectra that simultaneously provide DC and CS values for each labeled residue. Two-dimensional spectra of α -helices yield ellipsoidal resonance patterns called PISA (polar index slant angle) wheels. Since the tilt (τ) defines the pattern, shape, and size of the PISA wheels, determining the tilt does not require the assignment of the individual signals on the wheel. The rotation (ρ) is provided by indexing and, therefore, assigning the resonances on the wheel. 17-20 Alternatively, the DC and CS values from the 2D spectra can be plotted as a function of residue number and fitted with sinusoidal waves to obtain the orientation of the peptide (Figures 2.1A and 2.1B). The amplitude of the wave is related to τ and the phase is related to ρ . Since not only the orientation but also the periodicity of the α-helix is reflected in dipolar waves, dipolar wave-fit analysis can be used to reveal deviations from the ideal α -helix, such as kinks and bends. 21-25 When an α -helix is allowed to explore its full conformational space, its dipolar wave, CS wave, and PISA wheel are inherently related to each other, as demonstrated in Figure 2.1D. The gray 3D coil in the center of Figure 2.1D is determined by the orientations of the dipolar and chemical shift tensors with respect to the static magnetic field.

The orientation of membrane-bound peptides, as well as the DC and CS values of their individual peptide planes, can be independently and directly determined from MD simulations. At the beginning of this chapter, the calculation of DC and CS values from simulations and the derivation of the dipolar and CS waves are presented. Next, it is demonstrated that dipolar and CS waves may give inaccurate orientations or even multiple solutions when typical uncertainties in the experimental measurements are taken into account. Comparing orientations deduced from the dipolar wave to those sampled in MD can reduce this ambiguity. Since the NMR observables can be affected by peptide dynamics, the effect of dynamics on the order parameter of the NH bond and the implications for the rigorous determination of peptide structures are also discussed. Specifically, the bias in orientation due to peptide dynamics, such as fluctuations about the helical axis, is investigated. For a peptide with a fluctuation in $\tau > 20^{\circ}$, wave fitting may result in a τ -value that is not equal to the average τ obtainable by MD. Bringing into agreement the analyses of the NMR and MD data as presented here instills confidence in properties directly obtainable by MD but not NMR, such as the depth of insertion of the

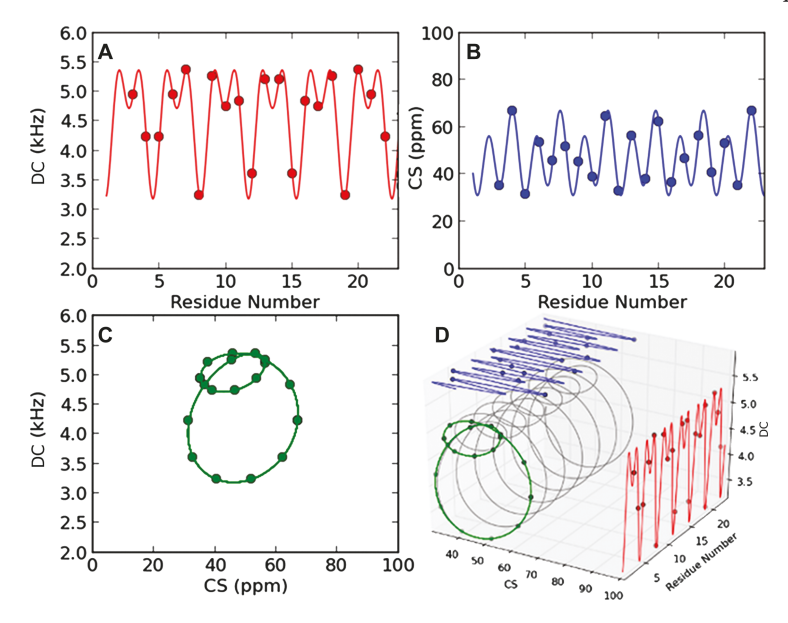


Figure 2.1 Examples of (A) a dipolar wave, (B) a chemical shift (CS) wave, and (C) a PISA wheel for an ideal α-helix $(\phi/\psi=-61^{\circ}/-45^{\circ})$ with $\tau=85^{\circ}$ and $\rho=260^{\circ}$. (D) 3D plot demonstrating the relationship between plots (A–C). The tilt, τ , determines the amplitude of the dipolar or CS waves and size of the PISA wheel, while the rotation, ρ , determines the phase of the waves. Intertwined wheels are observed in (C). Waves were generated using average $D_{\rm a}$ and principal elements for the ¹⁵N chemical shift tensor interaction.

peptide in the bilayer. The use of dipolar waves and MD simulations to assist in the assignment of DC signals from multiply labeled peptides is also presented.

In previous work,²⁶ the orientation of two antimicrobial amphipathic cationic peptides, piscidin 1 (p1, FFHHIFRGIVHVGKTIHRLVTG) and piscidin 3 (p3, FIHHIFRGIVHAGRSIGRFLTG), bound to oriented lipid bilayers that mimic bacterial cell membranes was studied with dipolar waves, CS waves, NMR structure refinement by Xplor-NIH,²⁷ and MD. Experimentally, these structural studies are particularly challenging because the orientation of amphipathic helices, almost parallel to the membrane surface, translates into crowded NMR spectra where the ¹⁵N chemical shifts and ¹⁵N–¹H dipolar couplings are smaller than 80 ppm and 11 kHz, respectively (Figure 2.2). Some of the results from the investigation of p1 and p3 are elaborated here to illustrate nuances of the aforementioned methods. While these examples more directly pertain to interfacial peptides, much is also applicable to TM peptides and proteins.

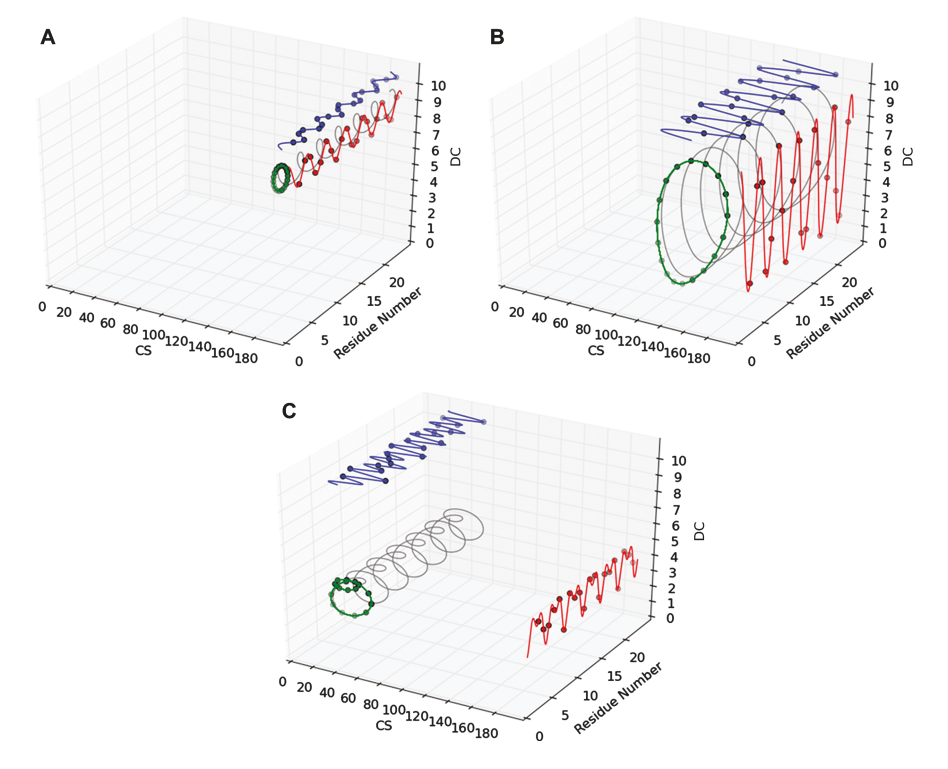


Figure 2.2 CS, DC, and residue number for an ideal 22-residue α-helix with (A) $\tau = 5^{\circ}$, (B) $\tau = 30^{\circ}$, and (C) $\tau = 85^{\circ}$; $\rho = 260^{\circ}$ for all plots.

2.2 Orientation of an α-Helix from ¹H-¹⁵N Dipolar Couplings and ¹⁵N Chemical Shifts

Since both the DC and CS interaction tensors are fixed with respect to the molecular frame but depend on their orientation relative to the static magnetic field, it is straightforward to express the orientation of the interaction tensors with respect to the helical axis and magnetic field. DC is calculated as:

$$DC = D_a \left\langle \frac{3\cos^2(\theta) - 1}{2} \right\rangle \tag{2.1}$$

where $D_{\rm a}$ is the static internuclear dipolar coupling magnitude $(D_{\rm a}=\mu_0\hbar\gamma_{\rm H}\gamma_{\rm N}/4\pi^2r_{\rm NH}^3)$, and θ is the angle of the NH vector with respect to the bilayer normal, \vec{n} (Figure 2.3). The ¹⁵N chemical shift is calculated as: 18,20

$$CS = \sigma_{11}\lambda_1^2 + \sigma_{22}\lambda_2^2 + \sigma_{33}\lambda_3^2$$
 (2.2)

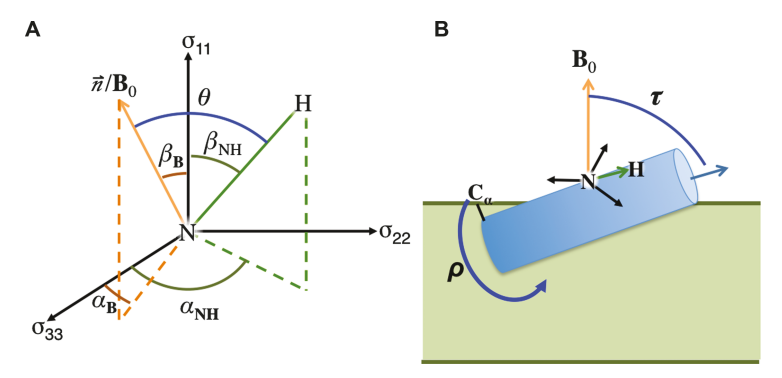


Figure 2.3 (A) Geometric relationship of the angles relating the 15 N– 1 H tensor and the principal axis frame of the 15 N chemical shift tensor to the static magnetic field. (B) Polar angles τ and ρ that define the orientation of an α-helix with respect to the helical axis and the static magnetic field. The N-terminus of the peptide is on the left-hand side. By convention, B_0 is along the z-axis of the orthogonal (x,y,z) coordinate system.

where σ_{11} , σ_{22} , and σ_{33} are the principal elements of the ¹⁵N chemical shift tensor interaction, and

$$\begin{split} \lambda_1 &= \sin(\beta_B) \cos(\alpha_B) \\ \lambda_2 &= \sin(\beta_B) \cos(\alpha_B) \\ \lambda_3 &= \cos(\beta_B) \end{split} \tag{2.3}$$

where $\alpha_{\rm B}$ is the angle between σ_{33} and the projection of \vec{n} onto the $\sigma_{22}\sigma_{33}$ plane, and $\beta_{\rm B}$ is the angle between σ_{11} and \vec{n} . This is illustrated in Figure 2.3A.

For an α -helix, DC is fit to a sinusoidal wave with a periodicity of 3.6 residues per turn, which restricts the values of θ . 22 θ oscillates between $\theta + \delta$ and $\theta - \delta$, where δ is the angle of the tensor principal axes for 15 N CS or 1 H- 15 N DC interactions in the molecular frame. θ is propagated along the length of the helical axis as:

$$\theta = \theta - \delta \cos(x\Omega) \tag{2.4}$$

where x is the residue number and Ω is the rotation angle per residue. DC becomes:

$$DC = D_a \left(\frac{3\cos^2(\theta - \delta\cos(x\Omega)) - 1}{2} \right)$$
 (2.5)

Equation (2.1) can also be derived for the orientation of the ${}^{1}\text{H}-{}^{15}\text{N}$ vector, *NH*, relative to the static magnetic field, B_0 :

$$DC = D_a \left[\frac{3(B_0 \cdot NH)^2 - 1}{2} \right]$$
 (2.6)

where

$$\mathbf{\textit{B}}_{0} = \begin{bmatrix} \sin(\beta_{B})\cos(\alpha_{B}) \\ \sin(\beta_{B})\sin(\alpha_{B}) \\ \cos(\beta_{B}) \end{bmatrix}, \mathbf{\textit{NH}} = \begin{bmatrix} \sin(\beta_{NH})\cos(\alpha_{NH}) \\ \sin(\beta_{NH})\sin(\alpha_{NH}) \\ \cos(\beta_{NH}) \end{bmatrix}$$
(2.7)

In the helical axis frame (HAF), $\alpha_{\rm NH} = 0^{\circ}$, $\beta_{\rm NH} = \angle {\rm CNH} - \beta_{\rm D} = \delta$, $\angle {\rm CNH} = 122^{\circ}$, and $\beta_{\rm D} = 105^{\circ}$, 28,29 resulting in an $\it NH$ that is related to the tilt of a peptide in a bilayer aligned such that the normal, $\vec n$, is parallel to the magnetic field (Figure 2.3). Therefore, Eqn (2.7) written in terms of $\tau(0 < \tau < 90)$ and $\rho(0 < \rho < 180)$ becomes:

$$\mathbf{B}_{0}^{\text{HAF}} = \begin{bmatrix} \sin(\tau)\cos(\rho - x\Omega) \\ \sin(\tau)\sin(\rho - x\Omega) \\ \cos(\tau) \end{bmatrix}, \mathbf{NH} = \begin{bmatrix} \sin\delta \\ 0 \\ \cos\delta \end{bmatrix}$$
(2.8)

where δ is 17° and Ω is 100°;¹⁵ however, δ and Ω can change significantly with ϕ and ψ . The preceding values for δ and Ω were for $\phi=-61^\circ$ and $\psi=-45^\circ$, as found for α -helices in most proteins. Equation (2.2) is solved relative to τ and ρ when:

$$\lambda_{1} = \sin(\tau)\cos(\rho - x\Omega)$$

$$\lambda_{2} = \sin(\tau)\sin(\rho - x\Omega)$$

$$\lambda_{3} = \cos(\tau)$$
(2.9)

Dipolar and CS waves are continuous plots in the HAF of DC or CS as a function of residue number along the α -helix. The wave is best fit to a set of DC or CS data by adjusting τ and ρ . DC and CS for the MD structures presented here were calculated using CHARMM 36b2. DC was determined from Eqn (2.1) with $D_{\rm a}=10.735$ kHz; and CS was calculated using the NMR facility with $^{15}{\rm N}$ chemical shift tensor principal elements of $\sigma_{11}=32$ ppm, $\sigma_{22}=54$ ppm, and $\sigma_{33}=202$ ppm referenced with respect to an aqueous solution of $^{15}{\rm N}$ -labeled ammonium sulfate. 19,20

The symmetry of nuclear spin interactions results in ambiguities when solving for the orientation of helices by OS ssNMR. Indeed, angles τ and $(180 - \tau)$ give rise to the same NMR resonances in uniaxially oriented samples. In addition, the sign of DC is uncertain when it is smaller than half the maximum value (10.735 kHz), as is the case in membrane-bound piscidin. However, simultaneously considering the DC and Indicates of piscidin indicates that its DC values are negative. When this sign is known, the number of ambiguities can be reduced to two orientations $(180-\tau,\rho)$ and τ , $180 + \rho$ of the helical axis, which are magnetically equivalent and consistent with the dipolar waves. However, only one combination yields a

peptide orientation such that the hydrophobic side chains are pointing toward the hydrophobic bilayer. The other combination, which directs hydrophilic side chains toward the core of the bilayer, is energetically unfavorable. Consequently, only the former orientation is considered in the rest of this chapter.

Motions affect the NMR observables, including the dipolar couplings and chemical shifts. ^{14,16,32,33} Therefore, the derivation of reliable structures from these variables requires investigating motional averaging in terms of rate, axis, and amplitude. Considering the amphipathic helix of piscidin, molecular motions include the diffusion of the peptide about the bilayer normal, ³⁴ which is aligned parallel to the static magnetic field, and the rocking of the peptide about its helical axis. In the aligned samples considered in this chapter, the helical axis is approximately perpendicular to the static magnetic field and, therefore, signal averaging arises mostly from the rocking motion as well as local motions around the torsion angles. As demonstrated previously through the comparison of NMR and MD data, ²⁶ and expanded upon in this chapter, the NMR observables collected for piscidin are reliable restraints for structural determination at high resolution.

2.3 Crosschecking ¹H-¹⁵N Dipolar Coupling Assignments of Multiply Labeled Peptides

The amide $^{15}N^{-1}H$ dipolar couplings for multiply labeled peptides are not straightforward to assign if the ^{15}N -amide sites have similar signals or the residue has multiple signals due to ^{15}N -containing side chains. Dipolar waves can help guide the selection of signals; however, the ability to fit the experimental data with a wave for short helical segments may become difficult because the experimental data points may not span a full period of the wave. Furthermore, kinks and bends in the helix distort the dipolar wave, and fraying at the termini may result in smaller than expected DC due to increased dynamics. In Figure 2.4, dipolar waves are fit to a set of DC for the 22-residue peptide p1 in 1:1 phosphatidylethanolamine/ phosphatidylglycerol (PE/PG). A glycine at position 13 adds flexibility and a kink to the peptide, necessitating a fit of residues 3–10 using $(\tau_{\rm N}, \rho_{\rm N})$ separately from residues 14 to 20 that are fitted using $(\tau_{\rm C}, \rho_{\rm C})$. Two residues at each terminus do not belong to the best-fit wave due to helical fraying.

In the process of fitting the experimental data of p1 in PE/PG to a kinked helix, Arg18 was initially assigned a DC of 1.9 kHz. MD simulations of the same peptide in the same bilayers predicted a DC of 4.8 kHz. This was a clear outlier as the other sites had experimental and simulated DC values that agreed within 1 kHz. Further inspection of the experimental data revealed the presence of another DC splitting at 5.1 kHz. Thanks to the MD predictions, the larger splitting could be confidently assigned to the backbone of Arg18.

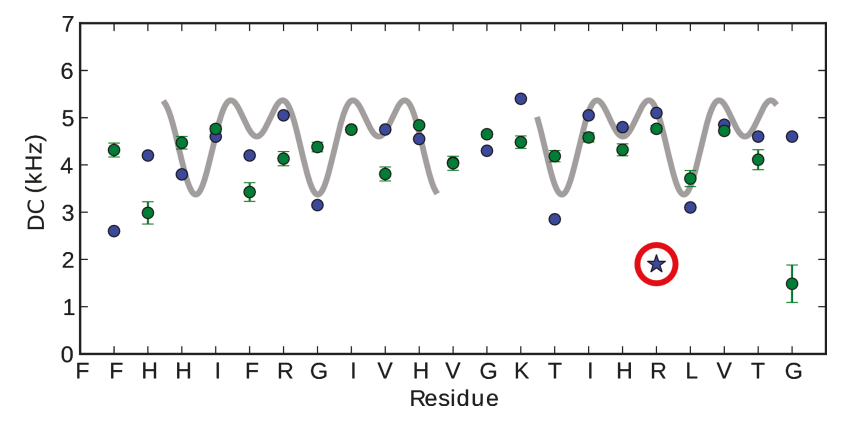


Figure 2.4 DC for piscidin 1 in PE/PG from ssNMR (*blue*) and MD (*green*). DC for the side chain of Arg18 is circled in *red*. Dipolar wave fits to the experimentally observed DC are shown in *gray* for an ideal α -helix, assuming dihedral angles ϕ of -61° and $\psi=-45^{\circ}$. A kink at position 13 is identified by the need to use different τ and ρ values to fit the experimental data at the N- and C-ends of the peptide. τ, ρ values of 86°, 251° and 83°, 248° were used at the N- and C-ends, respectively.

2.4 Inaccurate Orientations from Dipolar and Chemical Shift Waves

In some cases, the orientations determined from best-fit dipolar or CS waves are not accurate. This can be due to the wave fit yielding multiple (τ, ρ) solutions within the uncertainty of the measured DC or CS. The remainder of this section considers fitting of the dipolar and CS waves within experimental error. Two examples are provided: one for p1 in 3:1 phosphatidylcholine/phosphatidylglycerol (PC/PG) with a single expected solution; and one for p3 in 1:1 PE/PG with multiple solutions. Finally, the use of MD simulations to resolve the more likely value is presented.

Based on experimental linewidths, errors in the experimental DC (0.2 kHz) and CSA (3.0 ppm) were propagated into the dipolar and chemical shift waves from an ensemble of synthetic data. Specifically, 1000 sets of DC for the two examples were generated with the DC for each residue calculated as a random number from a Gaussian distribution with a mean equal to the measured values and a standard deviation (σ) of 0.2 kHz for DC and 3.0 ppm for CS. Dipolar or CS waves were fit to the DC or CS values for residues 3–10 or residues 14–20 by a Levenberg–Marquardt minimization. 35,36 For p3 in 1:1 PE/PG, which does not have an experimental DC for residue 3, the dipolar wave was fit to residues 4–10. Statistically, instances

where multiple solutions exist within the experimental error will be characterized by high standard deviations in the solution $(\sigma[\tau])$ or $\sigma[\rho]$.

2.4.1 Single-Solution Example: Orientation of Piscidin 1 in PC/PG

In the example of p1 in PC/PG, the 1000 waves for DC are tightly fit to one solution, as seen by the significant overlap (Figure 2.5A). Figure 2.5B shows a narrow band of solutions for τ_N and τ_C at 88° and 82°, respectively. The narrow range of solutions for τ_N and τ_C demonstrates the sensitivity of the dipolar waves to a change in τ and corroborates results on TM helices. ^{19,22} On the other hand, the solutions for ρ_N and ρ_C cover broad ranges of solutions with averages at 259° and 249°, respectively. This insensitivity to variation in ρ demonstrates the small effect that rotation around the helical axis has on the orientation of the amide bond, which is parallel to the helical axis and perpendicular to the magnetic field for interfacial helices in mechanically aligned samples. The NMR-derived values are comparable to those obtained by MD, specifically τ_N , ρ_N of 91°, 265° and τ_C , ρ_C of 87°, 245°. Therefore, this first example is characterized by an experimentally determined orientation that is accurate.

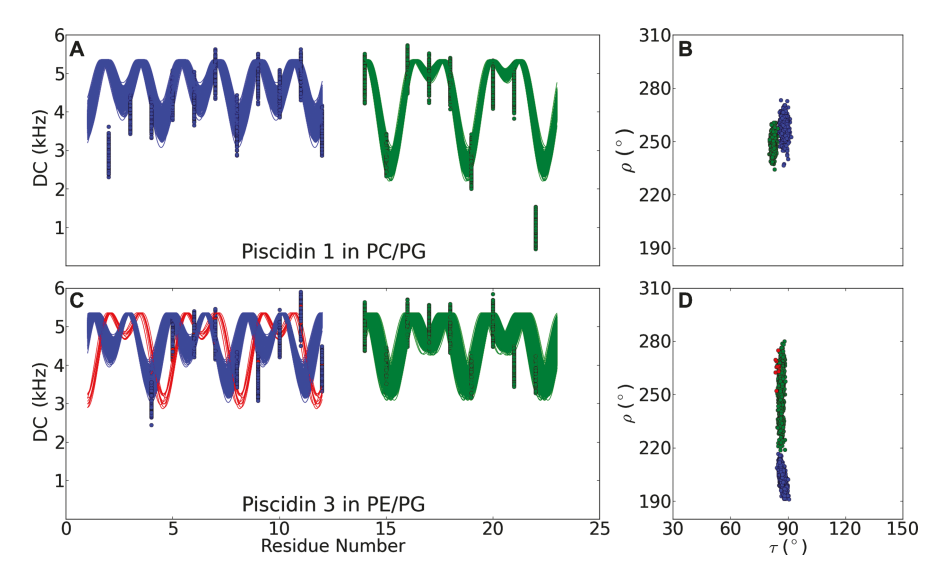


Figure 2.5 Dipolar wave fits to the 1000 sets of DC randomly selected from a Gaussian distribution with a mean equal to the experimental DC and $\sigma=0.2$ kHz. Simulated data for piscidin 1 in PC/PG and piscidin 3 in PE/PG are shown in (A) and (C), respectively. Corresponding τ and ρ values for the wave fits are plotted in (B) and (D). Orientations for residues 3 to 10 (4 to 10 for p3) are in *blue* and those for 14 to 20 are in *green*. Secondary solutions for residues 4 to 10 of piscidin 3 in PE/PG are shown in *red*.

2.4.2 Multiple-Solution Example: Orientation of Piscidin 3 in PE/PG

In the case of p3 in PE/PG, a straightforward solution for ρ could not be identified using wave fits. Figure 2.5C shows a narrow band of solutions for τ ; however, when $\rho_{\rm N}$ is considered, there are multiple solutions to the dipolar wave fit. One of these solutions has a $\rho_{\rm N}$ near 200° (blue in Figures 2.5C and 2.5D), while the second is closer to 260° degrees (red). In the simulated system, $\rho_{\rm N}$ is 241° with a root-mean squared fluctuation of 11°, while $\rho_{\rm N}$ is 250° for the NMR-derived wave and refined structure. This indicates that $\rho_{\rm N}=260^\circ$ rather than 200° is the likely solution.

Since the percent error in CS is higher than that in DC for in-plane helices, multiple solutions are more common for CS than DC wave-fit analysis. In Figure 2.6, which shows CS wave-fit analysis, multiple solutions for $\tau_{\rm N}$ and $\rho_{\rm N}$ are obtained for both p1 in PC/PG and p3 in PE/PG. Moreover, the solutions are clustered with τ,ρ of 82°, 240° or 100°, 260° for p1 and τ,ρ of 80°, 260° or 100°, 280° for p3. In both systems, the smaller solution for $\tau_{\rm N}$ is less than the values obtained by MD ($\tau_{\rm N},\rho_{\rm N}$ of 93°, 241°), while the larger solution is significantly too large to be in agreement with the dipolar waves and MD values. The discrepancy between solutions and difficulty in relying on experiments to obtain an accurate solution are likely due to the percent

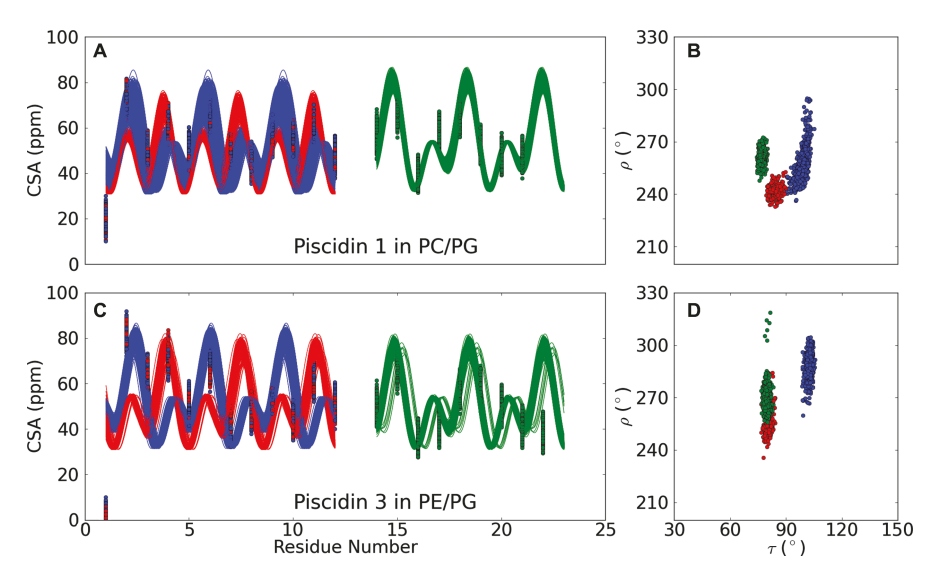


Figure 2.6 CS wave fits to the 1000 sets of CS randomly selected from a Gaussian distribution with a mean equal to the experimental CS and $\sigma=3.0$ ppm. Simulated data are shown for piscidin 1 in PC/PG and piscidin 3 in PE/PG in (A) and (C), respectively. Corresponding τ and ρ for the wave fits are plotted in (B) and (D). Orientations for residues 3 to 10 (4 to 10 for p3) are in *blue* and those for 14 to 20 are in *green*. Secondary solutions for residues 4 to 10 are shown in *red*.

error in the experimental CS and/or the use of a common ¹⁵N chemical shift tensor for all residues in the CS wave fits.

2.4.3 Resolving the Accurate Orientation with MD or Structural Refinement

MD simulations can help resolve the problem of multiple solutions in two ways. First, the sampling of wave-fits to points within the experimental error via a best-fit algorithm is the primary method for unbiased generation of solutions. In the aforementioned case of p3 in PE/PG, for which multiple solutions exist and differ in ρ by 50° , the difference between solutions is well within the range that can be resolved by a MD simulation of the peptide in the bilayer. While the experimental data alone do not yield an accurate solution in this example, combining NMR refinement and MD simulations resolves this issue and helps identify a τ, ρ combination in the vicinity of 90° , 250° .

2.4.4 Change to the Static Internuclear Dipolar Coupling and Anisotropic Order Parameter due to Peptide Dynamics

Proteins and peptides bound to bilayers are not rigid, and a rigorous determination of protein structure should include the effect of dynamics on the NMR variables.^{37,38} Specifically, when refining the structure of a peptide through simulated annealing the experimental order parameters (which are used as restraints) are commonly scaled to take into account experimental error, mosaic spread (residual sample disorder), and fast librations of the peptide. While experimental error and mosaic spread are not likely to be predicted from an atomistic simulation, reduction of order parameters by fast motions of the amides can be examined by MD.

Here, estimating this reduction of order parameters is based on $C_{20}(t)$, the correlation function of Y_{20} , the second-order spherical harmonic:

$$C_{20}(t) = \langle \mathbf{Y}_{20}(0) \mathbf{Y}_{20}(t) \rangle = \left\langle \left(\frac{3z^2(0) - 1}{2} \right) \left(\frac{3z^2(t) - 1}{2} \right) \right\rangle \tag{2.10}$$

where z(t) is the z-component of the unit vector along the N-H bond. The long-time or plateau value of $C_{20}(t)$ is:

$$C_{20}(t) = \left\langle \frac{3z^2 - 1}{2} \right\rangle^2 = \left(\frac{DC}{D_a}\right)^2 \tag{2.11}$$

The second equality follows from Eqn (2.1) and the definition $z = \cos \theta$.

Figure 2.7A shows plots of $C_{20}(t)$ for the NH vectors of residues 2 (toward the N-terminus), 8 (center of the helix), and 22 (the C-terminus) of p1 based on MD simulations in PC/PG;²⁶ Figure 2.7B shows the normalized

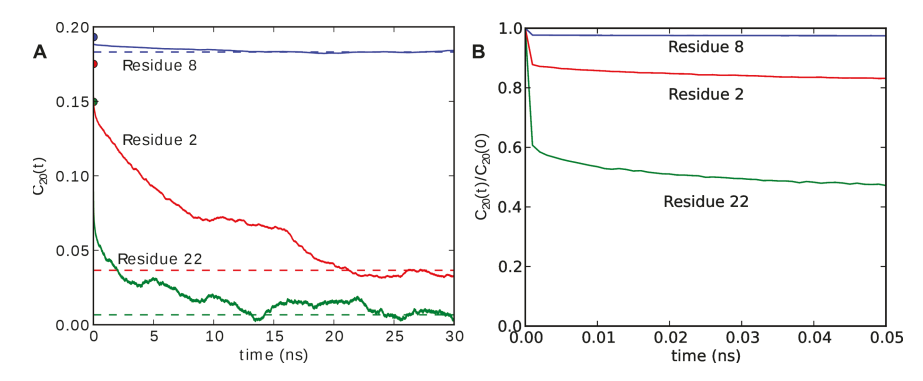


Figure 2.7 (A) Correlation function for the *z*-component of the amide bond for residues 2, 8, and 22; the *dashed lines* show $(DC/D_a)^2$ obtained as an average from the trajectory. (B) Normalized correlation functions from (A) at short times.

correlation function from 0 to 50 ps. It is clear that there are at least two exponential decays: a very rapid one on the ps timescale, and a slower one of approximately 5–10 ns. The former arises from fast internal motion, primarily libration in the torsional minima; the slower one arises from tilting motions of the helix. The dashed lines in Figure 2.7A show $(DC/D_a)^2$ obtained as an average from the trajectory, as opposed to from the correlation function. The confluence of order parameters calculated in these two ways is an important consistency check, and indicates that MD directly simulates the motions that modulate DC.

Returning to the fast motions, it is useful to write $C_{20}(t)$ as:

$$C_{j}(t) = S_{j}^{2} S_{s}^{2} + S_{j}^{2} (1 - S_{s}^{2}) \exp(-t/\tau_{s}) + (1 - S_{j})^{2} \exp(-t/\tau_{j})$$
 (2.12)

where the subscripts j and S denote correlation times and order parameters associated with fast motions (in principle different for each vector) and slow motions (common to all vectors), respectively.³⁹ S_j^2 is analogous to the "generalized order parameter" in the Lipari–Szabo treatment of solution NMR;⁴⁰ the observed order parameter is proportional to S_jS_S . S_j^2 can be obtained from fitting the simulated correlation function to Eqn (2.12) or, for the current example, simply read from Figure 2.7B: it is 0.98, 0.88, and 0.61 for residues 8, 2, and 22, respectively. As may be inferred from the large variation in the preceding S_j^2 , scaling observed dipolar couplings by a single constant could introduce errors in structural refinements.

2.5 Error in Measured Orientation due to Large Fluctuations in τ

Orientations of TM peptides obtained by NMR and MD have previously been shown to disagree. For WALP23, NMR gives tilt values of $\sim 5^{\circ}$ while the MD simulations predict a much larger tilt of $>30^{\circ}$. In the process of reproducing

the NMR observables from simulations of a rigid peptide fluctuating in τ , the PISA spectra were demonstrated to result in a bias of the average τ when fluctuations in τ were >20°. ¹⁰ This bias has been observed in experimental data consisting of CS, DC, and ²H quadrupolar splittings. ^{10,41} In this regard, specific approaches that have been scrutinized include the PISEMA experiment, which provides ¹⁵N CS and ¹⁵N–¹H DC, and the geometric analysis of labeled alanine (GALA) method, which relies on ²H quadrupolar splittings. This section demonstrates the bias in the context of the dipolar waves, CS waves, and PISA wheels.

The effect of fluctuations in τ and ρ can be incorporated into the DC and CS wave fits. To illustrate this effect, 1000 τ angles were randomly sampled from a Gaussian distribution of angles with a specified mean ("reference") τ and σ . The DC for each residue was averaged over each of the 1000 τ values. Next, each DC was averaged over the 1000 sets and dipolar waves were fit to the average DC values to give a fitted τ . The sampling was repeated for ρ and to fit CS, rather than DC. The mean range of τ values chosen here were between 0° and 90° with σ of 0°, 10°, and 20°, while the mean range of ρ values was between 180° and 270° with σ of 0°, 10°, 20°, and 40°.

Figure 2.8 shows the ensemble average orientation versus input ("reference τ, ρ "). It is clear that a peptide with fluctuations in $\tau \le 10^\circ$ or $\rho \le 20^\circ$ will have

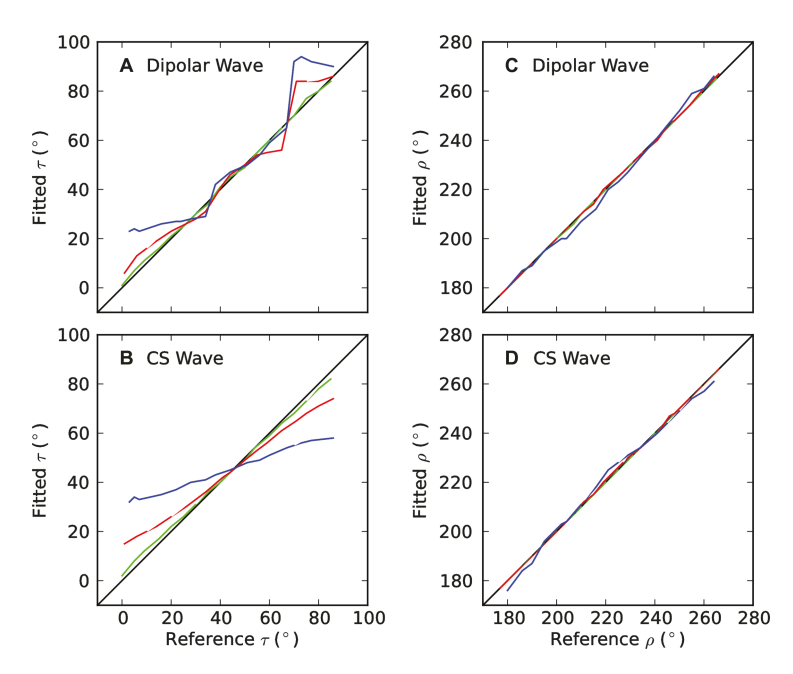


Figure 2.8 Fitted vs. reference (specified mean) values of τ and ρ with fluctuations of 10° (green), 20° (red), and 40° (blue). Fluctuations of 0° are equivalent to the black diagonal line, where fitted values are equal to the reference values. The further away the fitted values are from the diagonal, the less satisfactory is the fit.

an observed average similar to that of the ensemble average. However, fluctuations ${\geq}20^{\circ}$ result in a significant difference between ensemble and observed averages when τ is near 0° or 90° . In the case of piscidin, fluctuations ${<}10^{\circ}$ were observed and, therefore, the NMR structure is accurate. 26 It is likely that other amphipathic α -helical peptides in the monomeric state will have fluctuations similar to those of piscidin. These results are in agreement with those obtained by Esteban-Martín $et~al.,^{10}$ who calculated orientations by fitting a single reference peak with PISA wheels, which were simulated for different fluctuations around a mean tilt. The significance of the simulations presented here is that the individual bias in DC and CS can be characterized and that all amide bonds rather than a single reference peak were considered. Advantageously, using individual DC and CS values to plot PISA wheels, as done here, results in the expected two intertwined ellipses, as seen in Figure 2.1C, rather than the single ellipse shown in Esteban-Martín $et~al.^{10}$

2.6 Characterizing Atomistic Details not Directly Measurable by Solid-State NMR

The limitations of MD simulations include approximations in the force fields $^{42-44}$ and lack of temporal and spatial sampling. Hence, it is essential to compare simulation and experimental results before drawing conclusions from a trajectory. Where there is agreement between experiment and theory, the simulation can be used to investigate properties impossible or not easy to apprehend experimentally. For ssNMR, such properties include the depth of insertion of the peptide, membrane thinning, solvent accessibility to side chains, or structural deviations from ideality. The latter is important in peptides that include a kink or bend. As demonstrated here and alluded in previous work on piscidin, 26 dipolar and CS waves are unable to precisely determine small changes in τ and ρ . Therefore, small characteristics, such as the angle of a kink, may not be accurately determined; however MD simulations are very helpful in this regard. On another topic, the depth of insertion can be determined from either a long, equilibrated simulation or umbrella sampling at several specified depths of insertion.

MD simulations can also include restraints to determine the effect of different sample conditions. For instance, a peptide with ionizable residues can be simulated with different protonation states to examine possible effects on the peptide structure or orientation. Specifically, p1 contains four histidine residues and simulations of different charge states did not show significant differences in orientation with protonation of His3, 4, or 11. However, protonation of His17 in p1 caused a significant change in τ . ²⁶ This information may be used to predict peptide behavior as a function of pH.

2.7 Summary and Perspective

OS ssNMR provides crucial orientational restraints to elucidate the structure, orientation, and dynamics of peptides and proteins in lipid bilayers.

In this chapter, the focus was on in-plane α -helices that have not been as widely studied as TM helices. While ^{15}N CS and $^{15}N^{-1}H$ dipolar couplings were used here to investigate piscidin, the 2H quadrupolar splitting represents another orientational restraint that is available for assessing the conformational space of a peptide. In this regard, the GALA method relies on the geometrical analysis of 2H quadrupolar splittings from deuterated alanines to find τ and ρ values that agree with the experimental data. Typically, multiple alanine side chains are needed to specify a unique peptide topology. This approach requires that the peptide contain alanine residues and it is not possible to investigate the entirety of the peptide as needed to obtain an atomic-level structure and identify any distortion from ideality.

The complementarity of MD and OS ssNMR was illustrated in this chapter with the investigation of membrane-active piscidin. The orientation and fluctuations of piscidin in lipid bilayers that mimic bacterial cells have functional implications. For instance, the insertion of the peptide in the bilayer leads to disruptive effects such as membrane thinning and bending of the acyl chains. A detailed knowledge of peptide orientation and location in the bilayer is crucial to understanding its ability to perturb bilayers, form pores or micellar aggregates and ultimately lyse cells under native conditions. It has been shown for piscidin that varying the composition of the bilayer results in changes in peptide orientation and depth of insertion in the bilayer, and these effects are sequence dependent. In particular, increased anionic content of the bilayer results in less insertion in the bilayer and this may explain the lower activity of the peptide in bilayers that are more anionic.²⁶

MD simulations provide time-resolved descriptions of a system that benefit NMR experiments by corroborating results, reducing ambiguities, and identifying difficult-to-measure properties. MD simulations are becoming more accessible through webservers such as CHARMM-GUI⁴⁶ and CHARMMing,⁴⁷ and programs such as VMD.⁴⁸ In addition, computer hardware and faster algorithms are allowing MD simulations to reach the scales of microsecond on current supercomputers or even milliseconds on specialized hardware, such as Anton. 49 This increased accessibility allows experimentalists to fit their data to a mathematical model, which can be visualized and manipulated to improve intuition about the system, reduce incorrect assumptions, and result in more precise hypotheses for future testing. A limitation is that force field parameters may not exist for a molecule of interest. These parameters are based on gas phase quantum mechanical calculations, which derive bond lengths, angles, and point charges for the atoms, followed by liquid state simulations of model compounds. Attempts have been made to automate the process through webservers or programs. One example is ParamChem, which produces topology and parameter files for the CHARMM General Force Field.⁵⁰ In addition to parameterizing a molecule, it also selects atom and residue identifiers that do not conflict with preexisting parameters.

In conclusion, specific examples have been presented here to illustrate the advantages of combining OS ssNMR and MD to investigate membrane-bound peptides. The agreement of simulation and experiment for DC and CS provides a validation of the simulation, while agreement for orientation arguably confirms inferences from experiment. Furthermore, results from the two methods that are cross-validated support the use of MD to determine physicochemical properties of the peptide and lipids that are not directly or easily accessible experimentally. The accuracy of the atomic-level orientation achievable by this approach is attractive for study of a plethora of peptides and proteins that are active at lipid membranes.

References

- 1. S. Ozdirekcan, C. Etchebest, J. A. Killian and P. F. J. Fuchs, *J. Am. Chem. Soc.*, 2007, **129**, 15174.
- 2. S. K. Straus, W. R. P. Scott and A. Watts, J. Biomol. NMR, 2003, 26, 283.
- 3. I. Chandrasekhar, W. F. van Gunsteren, G. Zandomeneghi, P. T. F. Williamson and B. H. Meier, *J. Am. Chem. Soc.*, 2006, **128**, 159.
- 4. S. K. Kandasamy, D.-K. Lee, R. P. R. Nanga, J. Xu, J. S. Santos, R. G. Larson and A. Ramamoorthy, *Biochim. Biophys. Acta*, 2009, 1788, 686.
- 5. L. Shi, A. Cembran, J. Gao and G. Veglia, Biophys. J., 2009, 96, 3648.
- 6. Y. H. Lam, A. Hung, R. S. Norton, F. Separovic and A. Watts, *Proteins*, 2010, 78, 858.
- 7. A. Vogel, G. Reuther, M. B. Roark, K.-T. Tan, H. Waldmann, S. E. Feller and D. Huster, *Biochim. Biophys. Acta*, 2010, **1798**, 275.
- 8. A. Holt, L. Rougier, V. Réat, F. Jolibois, O. Saurel, J. Czaplicki, J. A. Killian and A. Milon, *Biophys. J.*, 2010, **98**, 1864.
- 9. A. Ramamoorthy, S. K. Kandasamy, D.-K. Lee, S. Kidambi and R. G. Larson, *Biochemistry*, 2007, **46**, 965.
- 10. S. Esteban-Martín, E. Strandberg, G. Fuertes, A. S. Ulrich and J. Salgado, *Biophys. J.*, 2009, **96**, 3233.
- 11. M. Weingarth, C. Ader, A. J. S. Melquiond, D. Nand, O. Pongs, S. Becker, A. Bonvin and M. Baldus, *Biophys. J.*, 2012, **103**, 29.
- 12. S. Jo and W. Im, Biophys. J., 2011, 100, 2913.
- 13. C. H. Wu, A. Ramamoorthy and S. J. Opella, *J. Magn. Reson., Ser. A*, 1994, **109**, 270.
- 14. R. Fu and T. A. Cross, Annu. Rev. Biophys. Biomol. Struct., 1999, 28, 235.
- 15. S. J. Opella and F. M. Marassi, Chem. Rev., 2004, 104, 3587.
- 16. F. M. Marassi, B. B. Das, G. J. Lu, H. J. Nothnagel, S. H. Park, W. S. Son, Y. Tian and S. J. Opella, *Methods*, 2011, 55, 363.
- 17. F. M. Marassi and S. J. Opella, J. Magn. Reson., 2000, 144, 150.
- 18. F. M. Marassi and S. J. Opella, J. Biomol. NMR, 2002, 23, 239.
- 19. J. Wang, J. Denny, C. Tian, S. Kim, Y. Mo, F. Kovacs, Z. Song, K. Nishimura, Z. Gan, R. Fu, J. R. Quine and T. A. Cross, *J. Magn. Reson.*, 2000, 144, 162.

 J. K. Denny, J. Wang, T. A. Cross and J. R. Quine, J. Magn. Reson., 2001, 152, 217.

- 21. A. A. Nevzorov, M. F. Mesleh and S. J. Opella, *Magn. Reson. Chem.*, 2004, **42**, 162.
- 22. M. F. Mesleh and S. J. Opella, J. Magn. Reson., 2003, 163, 288.
- 23. M. F. Mesleh, S. Lee, G. Veglia, D. S. Thiriot, F. M. Marassi and S. J. Opella, *J. Am. Chem. Soc.*, 2003, **125**, 8928.
- 24. S. Kim and T. A. Cross, J. Magn. Reson., 2004, 168, 187.
- 25. R. C. Page, S. Kim and T. A. Cross, Structure, 2008, 16, 787.
- 26. B. S. Perrin Jr., Y. Tian, R. Fu, C. V. Grant, E. Y. Chekmenev, W. E. Wieczorek, A. E. Dao, R. M. Hayden, C. M. Burzynski, R. M. Venable, M. Sharma, S. J. Opella, R. W. Pastor, M. L. Cotten, DOI: 10.1021/ja411119m.
- 27. C. D. Schwieters, J. J. Kuszewski, N. Tjandra and G. M. Clore, *J. Magn. Reson.*, 2003, **160**, 65.
- 28. W. Mai, W. Hu, C. Wang and T. A. Cross, Protein Sci., 1993, 2, 532.
- 29. Q. Teng and T. A. Cross, J. Magn. Reson., 1989, 85, 439.
- B. R. Brooks, C. L. Brooks III, A. D. MacKerell Jr, L. Nilsson, R. J. Petrella,
 B. Roux, Y. Won, G. Archontis, C. Bartels, S. Boresch, A. Caflisch,
 L. Caves, Q. Cui, A. R. Dinner, M. Feig, S. Fischer, J. Gao, M. Hodoscek,
 W. Im, K. Kuczera, T. Lazaridis, J. Ma, V. Ovchinnikov, E. Paci,
 R. W. Pastor, C. B. Post, J. Z. Pu, M. Schaefer, B. Tidor, R. M. Venable,
 H. L. Woodcock, X. Wu, W. Yang, D. M. York and M. Karplus, J. Comput.
 Chem., 2009, 30, 1545.
- 31. R. Bertram, T. Asbury, F. Fabiola, J. R. Quine, T. A. Cross and M. S. Chapman, *J. Magn. Reson.*, 2003, **163**, 300.
- 32. S. H. Park, A. A. Mrse, A. A. Nevzorov, A. A. De Angelis and S. J. Opella, *J. Magn. Reson.*, 2006, **178**, 162.
- 33. R. R. Ketchem, W. Hu and T. A. Cross, Science, 1993, 261, 1457.
- 34. E. Chekmenev, B. Vollmar and M. Cotten, *Biochim. Biophys. Acta*, 2010, 1798, 228.
- 35. K. Levenberg, Q. Appl. Math., 1944, 2, 164.
- 36. D. Marquardt, SIAM J. Appl. Math., 1963, 11, 431.
- 37. R. Ishima and D. A. Torchia, Nat. Struct. Biol., 2000, 7, 740.
- 38. G. Bouvignies, P. R. L. Markwick and M. Blackledge, *ChemPhysChem*, 2007, **8**, 1901.
- 39. R. W. Pastor, R. M. Venable, M. Karplus and A. Szabo, *J. Chem. Phys.*, 1988, **89**, 1128.
- 40. G. Lipari and A. Szabo, J. Am. Chem. Soc., 1982, 104, 4546.
- 41. W. Im, S. Jo and T. Kim, Biochim. Biophys. Acta, 2012, 1818, 252.
- 42. J. B. Klauda, R. M. Venable, A. D. MacKerell Jr. and R. W. Pastor, *Curr. Topics Membr.*, 2008, **60**, 1.
- 43. O. Guvench and A. D. MacKerell, Methods Mol. Biol., 2008, 443, 63.
- 44. R. W. Pastor and A. D. MacKerell, J. Phys. Chem. Lett., 2011, 2, 1526.
- 45. B. Bechinger and E. S. Salnikov, Chem. Phys. Lipids, 2012, 165, 282.
- 46. S. Jo, T. Kim, V. G. Iyer and W. Im, J. Comput. Chem., 2008, 29, 1859.

- 47. B. T. Miller, R. P. Singh, J. B. Klauda, M. Hodošček, B. R. Brooks and H. L. Woodcock, *J. Chem. Inf. Model.*, 2008, 48, 1920.
- 48. W. Humphrey, A. Dalke and K. Schulten, *J. Mol. Graphics*, 1996, 14, 33–38.
- 49. E. Shaw, M. M. Deneroff, R. O. Dror, J. S. Kuskin, R. H. Larson, J. K. Salmon, C. Young, B. Batson, K. J. Bowers, J. C. Chao, M. P. Eastwood, J. Gagliardo, J. P. Grossman, C. R. Ho, D. J. Ierardi, I. Kolossvary, J. L. Klepeis, T. Layman, C. McLeavey, M. A. Moraes, R. Mueller, E. C. Priest, Y. Shan, J. Spengler, M. Theobald, B. Towles and S. C. Wang, in *Proceedings of the 34th Annual International Symposium on Computer Architecture*, ACM, San Diego, CA, 2007, p. 1.
- 50. K. Vanommeslaeghe, E. Hatcher, C. Acharya, S. Kundu, S. Zhong, J. Shim, E. Darian, O. Guvench, P. Lopes, I. Vorobyov and A. D. MacKerell Jr., *J. Comput. Chem.*, 2010, 31, 671.